

Modeling of articular cartilage replacement materials

M. STOFFEL¹⁾, D. WEICHERT¹⁾, R. MÜLLER–RATH²⁾

¹⁾*Institute of General Mechanics
RWTH Aachen, Germany
e-mail: stoffel@iam.rwth-aachen.de*

²⁾*Department for Orthopaedics and Trauma Surgery
RWTH Aachen, Germany*

THE DEVELOPMENT OF replacement material for human articular cartilage exhibiting similar mechanical properties as the native tissue is a problem of high actuality in biomedicine. In the present work a new condensed collagen material is investigated. The study aims at developing a mechanical model especially adapted to this particular collagen material. For this purpose, a viscoelastic-diffusion (VED) model is proposed, accounting for two different diffusion evolutions assumed. Moreover, the need for a gradient material description is discussed in order to cover fabrication influences leading to a variable Young's modulus for the material. On this background, a phenomenological law is presented to predict deformation-dependent diffusion behavior and internal reaction forces. Furthermore, the present approach allows a practicable identification of diffusion parameters. The theoretical model is implemented into a finite element code and parameters are identified by tension tests. The simulation results are validated experimentally.

Key words: diffusion model, viscoelasticity, material testing, finite element simulation.

Copyright © 2009 by IPPT PAN

1. Introduction

COLLAGEN IS A BASIC MATERIAL of human articular cartilage and the replacement material, used in the present study, is produced on the basis of water-saturated collagen gel. This material is very soft and has to be condensed in order to obtain the requested properties. Due to the condensation process, the mechanical properties of the soft material are strongly graded.

The aim of this study is to develop an appropriate model for assessing the applicability of this particular material by means of numerical simulations and a procedure how to determine experimentally the according material parameters. Special attention is placed on the damping and relaxation effects which are important for the use as a cartilage replacement tissue. In contrast to other models available in literature, a viscoelastic-diffusion (VED) model is proposed on a phenomenological basis allowing to predict internal forces and deforma-

tions of the used collagen material under close-to-service loading conditions. The leading idea for the presented model is to introduce only the material parameters to be identified by means of simple tension tests and finite element simulations. This way, deformation-dependent diffusion properties can be determined easily.

The present investigation focuses on three goals: The first one is the development of a strain rate-dependent tensor formulation for viscoelasticity and diffusion, which is necessary for the VED model in a phenomenological manner. The deformation-dependent diffusion is described by two different evolution equations with varying diffusion parameters. This accounts for the volume change due to the loss of water. In contrast to many other studies in literature, the present investigation accounts for the change of the Young's modulus in the material due to fabrication influences. The second goal is to derive an incremental formulation of the material law followed by an implementation into a finite element code. The third goal is to develop an experimental set-up for identifying material parameters and for validating the simulated results. Here, clamping devices for tension tests are constructed in order to identify material parameters and unconfined compression experiments are carried out to validate the proposed model.

Soft tissues like articular cartilage and replacement tissues can be interpreted as water-saturated bi-phasic materials. Many studies have been carried out to apply biphasic models to this type of soft material by separating solid and liquid from each other. Such an approach was proposed by EHLERS and MARKERT [1] based on the theory of porous media. DI SILVESTRO *et al.* [2] applied the theory of biphasic poroviscoelastic models (BPVE) to predict reaction forces in compression of articular cartilage. A nonlinear biphasic viscohyperelastic model was proposed by GARCÍA and CORTÉS [3] and continued by implementing the effect of fibres in [4]. Moreover, the swelling of cartilage was taken into account by a fibril-reinforced poroviscoelastic swelling model (FPVES) by WILSON *et al.* [5]. A refined numerical method for the BPVE model was developed by HAIDER and SCHUGART [6] using a discrete spectrum approximation in finite element simulations. GUILAK and MOW [7] implemented the mechanical behavior of chondrocytes as spheroidal inclusions in the framework of a biphasic finite element model. Also torsion moments were subjected to biphasic materials by MENG *et al.* [8].

The relaxation of the material as a very important property due to the damping function in human joints, is covered by the permeability of the propagating water through the pores. However, the identification of the material parameters, e.g. permeability coefficient or solid viscosity, is difficult and different methods have been reported to determine these parameters from experiments (MOW *et al.* [9], JOHNSON and DEEN [10], GU *et al.* [11]). Material coefficients for a fibril-reinforced poroelastic model were determined by LEI and SZERI [12].

A material parameter identification method based on the BPVE theory was developed for agarose hydrogel by OLBERDING and SUH [13].

A crucial point is the identification of deformation-dependent diffusion properties. Several attempts were made, e.g. by HOLMES and MOW [14], EHLERS and MARKERT [1], GU *et al.* [11], to determine diffusion coefficients connected with volume fraction of fluid and solid. In the present study, an alternative approach is proposed by applying a diffusion parameter depending on the volume strain. This model contains two diffusion coefficients to be identified from a tension test and by means of a finite element simulation.

Phenomenological models accounting for material properties such as anisotropy or viscoelastic damping were proposed in literature. In order to develop artificial tissues exhibiting anisotropic material behaviors, scaffolds were designed by COURTNEY *et al.* [15] and a phenomenological structural model was proposed. Similarly, fiber orientations in collagens were taken into account by means of scaffold microstructures in works of ENGELMAYR JR. *et al.* [16]. A linear solid viscoelastic model for determining the fracture load of soft tissues was proposed by KOOP and LEWIS [17]. A finite strain damage model for fibrous soft tissues was developed by RODRÍGUEZ *et al.* [18], based on a strain energy function. Damage of matrix and fibres are modeled separately also during softening. Other models using strain energy functions have been proposed also for different kinds of soft tissues, e.g. FUNG [19], HOLZAPFEL *et al.* [20]. EHRET and ITSKOV [21] derived a hyperelastic model for fiber-reinforced soft tissues using a polyconvex strain energy function. A finite element formulation based on an experimentally obtained strain energy function is derived by WEINBERG and KAAZEMPUR-MOFRAD [22] and applied for mitral valve leaflet tissues. The anisotropy due to fiber distribution has also been analyzed by BISCHOFF [23]. A variational constitutive finite strain model for soft tissues was presented by SAYED *et al.* [24] accounting for elasticity, plasticity, viscosity as well as for rate effects. The model is applied to experiments with brain tissues, allowing to identify model parameters. ZHANG *et al.* [25] proposed a generalized Maxwell model to predict hysteresis behavior of soft tissues and free model parameters were determined by experiments. A layered model with application for failure of arteries was presented by VOLOKH [26]. The fluid transport through the matrix is essential for the damping properties of the tissue. A model correlating microstructural anisotropy of the matrix with fluid transport, yielding a diffusion anisotropy, was derived by ZHANG and SZERI [27].

For material parameter identification procedures, tension tests with brain tissues were presented by MILLER and CHINZEI [28]. In order to avoid common problems of gripping soft tissues in tension tests, LEPETIT *et al.* [29] developed a cryogenic holder. By this method the ends of the samples are frozen by liquid

nitrogen. The effect of friction in unconfined compression tests for parameter identification was investigated by WU *et al.* [30]. JAQUEMOUD *et al.* [31] used tensile skin specimens to determine failure loads at different strain rates. Simple-shear experiments were conducted by GUO *et al.* [32]. KLEIN *et al.* [33] investigated depth-dependent mechanical properties of articular cartilage by compressive tests. Dynamic tests with soft human tissues using the Kolsky bar technique were carried out by SARAF *et al.* [34] who considered compression and shear loadings. In order to use a force spectrum in material parameter identification tests which represent the magnitude of physiological forces, it is important, especially if articular cartilage is regarded, to determine reaction forces in the human knee as KOEHLE and HULL [35] described. The problem of slipping during compression tests was described by MILLER [36] who used surgical glue leading to semi-confined experiments to avoid this effect.

In the present study, the material is modeled as an initially homogenous material exhibiting induced anisotropies due to strain-rate-dependent elasticity and diffusion. A fundamental principle, as described in Sec. 2, of the present investigation is that only these phenomena are implemented in the theoretical model which can be proved in the experiments. Otherwise the assumptions made in the mechanical model could not be validated. Due to the experimental observation of pure linear elasticity in tension tests, a linear elasticity model is used, see Sec. 2. However, the authors are aware of the fact that artificial tissues can exhibit material non-linearities. Nevertheless, in the present study, non-linear deformation histories, e.g. in compression tests, can be caused by superposition of the used linear elasticity with non-linear strain rate-dependence as well as with non-linear diffusion evolution. Geometrical non-linearities are covered by the applied finite strain model.

2. Methods and limitations of the study

The originally liquid material, composed of collagen and water, has to be condensed in order to obtain solid material properties. In the present study, the condensed material exhibits the twentieth of the volume in uncondensed form. During this process, liquid is pressed out of the water-collagen mixture and a water-saturated material remains.

The condensed material is fabricated in thin bands with plate geometry. The specimens are then cut out of the bands by means of stamping tools. However, due to the fabrication, the material composition of the specimens is not homogenous. They have a weaker core with a higher liquid concentration in contrast to a stiffer and dryer outer zone. Therefore, the specimens are treated as a gradient material with a Young's modulus varying from inside to outside of the specimen, see Fig. 1. Damage evolution or plasticity is not included in the

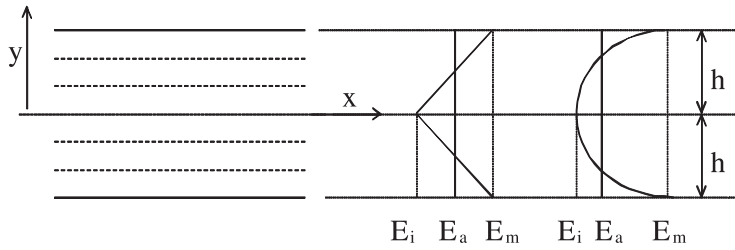


FIG. 1. Distribution of the Young's Modulus through the thickness of the specimen.

viscoelastic-diffusion model. However, the applied theory is also valid for finite strains as shown in Sec. 3.

For the numerical simulations, the finite element program Abaqus together with a user-defined subroutine is used. The theoretical model, described in Sec. 3, is implemented by means of the subroutine Vumat for explicit dynamic analyses.

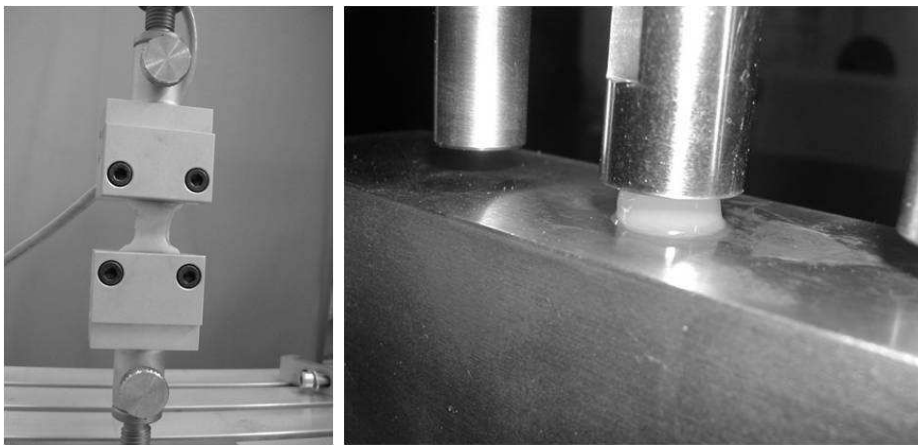


FIG. 2. Tension and compression experiments.

Tests are carried out on a MTS material testing machine. In Fig. 2 typical tension and compression experiments are shown. The compressive specimens have cylindrical forms with 2–3 mm thickness and 10 mm diameter. The tension specimens have the same thickness as the compression samples. Their active length between the clamping devices is 16 mm with 10 mm width. The tension specimens are additionally glued inside the clamping area and the clamping device is carefully screwed to avoid damage of the specimens, see Fig. 3. The tension and compression experiments were performed with displacement velocities of 0.005 mm/s, 0.05 mm/s and 0.5 mm/s. In order to cover scattering, all

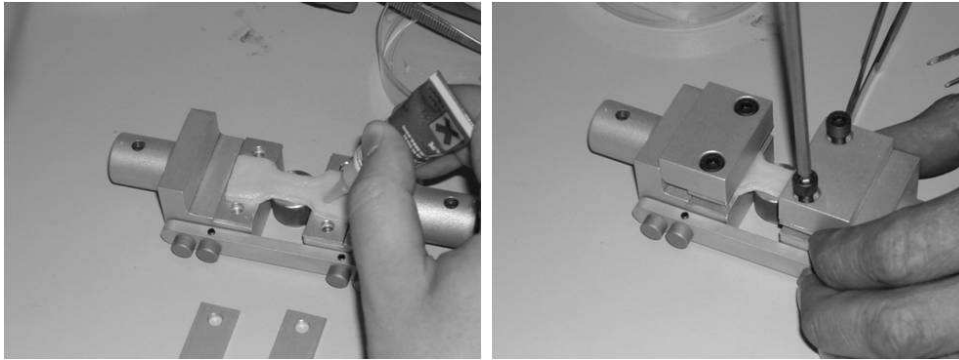


FIG. 3. Preparation of tensile specimens with glue and clamping device.

experiments were carried out three times with new samples. In numerical simulations with compression specimens, strains up to 0.3 occurred locally in the core and in the midsurface with maximum strain rates of 0.3/s. In the other regions strains smaller than 0.1 were distributed.

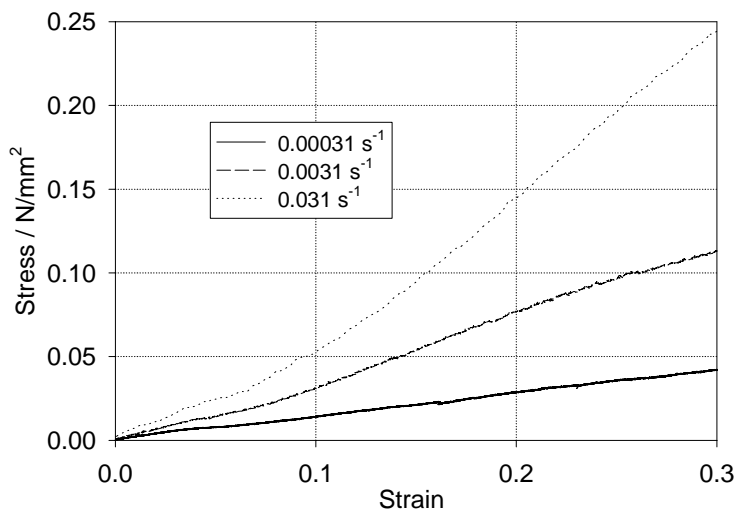


FIG. 4. Tension tests at different strain rates.

In order to identify the material parameters, tension tests are carried out with different strain rates, see Fig. 4, in the same interval of strains and strain rates as they occur in the simulations. The diffusion coefficient D_0 is also obtained by tension tests, while the parameter D_1 is identified by finite element simulations. The type of the Young's modulus distribution in the specimen, lin-

ear or quadratic, through the thickness and its internal value E_i are obtained by adapting the peak force in the measurement to the calculated one. Due to fabrication influences, the distribution of the Young's modulus through the specimen thickness has to be determined for each specimen.

3. Theoretical model

3.1. Basic principles

In the present study, the Eulerian description of strains and stresses is adopted. The deformation gradient is expressed as

$$(3.1) \quad F_{ij} = \frac{dx_i}{dX_j},$$

with x_i , X_j denoting the position of a particle in the current and reference configuration, respectively. Consequently, the total strain tensor for finite strains, accounting for geometrical non-linearities, can be written as

$$(3.2) \quad \varepsilon_{ij} = \frac{1}{2} \left(\delta_{ij} - F_{ki}^{-1} F_{kj}^{-1} \right),$$

with δ_{ij} standing for Kronecker's delta.

The velocity of a particle in Eulerian description is expressed as

$$(3.3) \quad v_i = \frac{\partial x_i}{\partial t},$$

with x_i denoting the position of a particle in the current configuration differentiated with respect to the time t . In order to determine the strain rate, a velocity gradient can be defined as

$$(3.4) \quad L_{ij} = \frac{\partial v_i}{\partial x_j},$$

and by means of Eq. (3.3) the velocity gradient can be expressed in terms of the deformation gradient as

$$(3.5) \quad L_{ij} = \dot{F}_{ij} \cdot F_{ij}^{-1},$$

with $\dot{(\)}$ denoting the time derivation. Following a decomposition of the L_{ij} into a deformation rate tensor and a spin tensor, the strain rate is obtained as

$$(3.6) \quad \dot{\varepsilon}_{ij} = \frac{1}{2} (L_{ij} + L_{ij}^T) = \frac{1}{2} \left(\left[\frac{\partial v_i}{\partial x_j} \right] + \left[\frac{\partial v_j}{\partial x_i} \right]^T \right)$$

and the antisymmetric spin tensor as

$$(3.7) \quad W_{ij} = \frac{1}{2} (L_{ij} - L_{ij}^T) = \frac{1}{2} \left(\left[\frac{\partial v_i}{\partial x_j} \right] - \left[\frac{\partial v_j}{\partial x_i} \right]^T \right).$$

Corresponding to the true strains in the current configuration, the Cauchy stress tensor σ_{ij} with true stresses is introduced for the equilibrium condition in the form

$$(3.8) \quad \int_S n_i \sigma_{ij} dS + \int_V f_j dV = 0,$$

with n_i and f_j as the unit outward normal vector to the surface S and the body force per unit of current volume V .

For the constitutive equations we need to define an objective stress rate. For this reason, we decompose the deformation gradient in a rigid body rotation, described by R_{kj} and the left stretch tensor V_{ik} , in the form

$$(3.9) \quad F_{ij} = V_{ik} R_{kj}.$$

A rotation of a convective base vector system in a material point can now be expressed by

$$(3.10) \quad \Omega_{ij} = \dot{R}_{ik} R_{kj}^T$$

leading to the Green–Nagdhi rate of the Cauchy stress tensor:

$$(3.11) \quad \sigma_{ij}^G = \dot{\sigma}_{ij} - \Omega_{ik} \sigma_{kj} + \sigma_{ik} \Omega_{kj}.$$

In the experiments with soft tissues, carried out in the present study, three material properties are observed: elasticity, superposed strain-rate dependence of material stiffness and relaxation. These effects are described by Eqs. (3.12)–(3.28). It is assumed, that the total stress rate tensor can be expressed by

$$(3.12) \quad \dot{\sigma}_{ij} = \dot{\sigma}_{ij}^e + \dot{\sigma}_{ij}^{ve} + \dot{\sigma}_{ij}^d,$$

where the upper indices e , ve , and d denote the elastic, viscoelastic and diffusion parts, respectively. The elastic behaviour is covered by Hooke's law

$$(3.13) \quad \dot{\sigma}_{ij}^e = C_{ijkl} \dot{\varepsilon}_{kl}$$

with C_{ijkl} as a matrix of elastic coefficients and ε_{kl} as a strain tensor. The viscoelastic material behavior is described by a rational function of the strain rate tensor

$$(3.14) \quad \dot{\sigma}_{ij}^{ve} = \tilde{C}_{ijkl}(\dot{\underline{\varepsilon}}) \dot{\varepsilon}_{kl}.$$

In the special one-dimensional case we assume

$$(3.15) \quad \sigma_{11}^{ve} = a\dot{\varepsilon}_{11}^v \varepsilon_{11},$$

where the values a and v are viscous material parameters.

3.2. Diffusion model VED1

In a relaxation process, the kind of a decreasing stress can be expressed by an exponential function for the one-dimensional case by

$$(3.16) \quad \sigma_{11} = Ae^{-Dt},$$

with A and D denoting free coefficients and t standing for the time, with $t = 0$ at the instant when relaxation starts. In order to transform this expression into an evolution equation, the exponential function is differentiated with respect to the time t

$$(3.17) \quad \dot{\sigma}_{11} = -DAe^{-Dt}$$

and inserted back in Eq. (3.16), leading to

$$(3.18) \quad \dot{\sigma}_{11} = -D\sigma_{11}.$$

Equation (3.18) is the necessary evolution equation which is used in tensor form

$$(3.19) \quad \dot{\sigma}_{ij} = -D\sigma_{ij}$$

for the diffusion process. It can be implemented as shown in Sec. 4 in a finite element code.

3.3. Diffusion model VED2

Another exponential function was proposed by BETTEN [37] for the one-dimensional case in order to improve the prediction of a relaxation process. This function is called the ‘ \sqrt{t} -law’ and is expressed by

$$(3.20) \quad \sigma_{11} = Ae^{-D\sqrt{t}}.$$

In the present study this law is transformed into an evolution equation for a three-dimensional analysis. Differentiating Eq. (3.20) and substituting in Eq. (3.20) leads to

$$(3.21) \quad \dot{\sigma}_{11} = -\frac{D}{2\sqrt{t}}\sigma_{11},$$

still including the time t . But by transforming Eq. (3.20) to

$$(3.22) \quad \sqrt{t} = -\frac{1}{D} \ln \left[\frac{\sigma_{11}}{A} \right]$$

and inserting in Eq. (3.21) the time derivative reads

$$(3.23) \quad \dot{\sigma}_{11} = \frac{1}{2} D^2 \frac{\sigma_{11}}{\ln \left[\frac{\sigma_{11}}{A} \right]},$$

exhibiting the form of an evolution equation. However, in Eq. (3.23) the parameter A is still undefined. In a one-dimensional deformation, A represents the maximum stress during the relaxation process. The question arises, which value the parameter A has to take in the three-dimensional case. Following the physical interpretation of a peak stress at time $t = 0$ in Eq. (3.20), as a counterpart in a three-dimensional case, the second invariant of the stress tensor σ_{ij} is chosen:

$$(3.24) \quad A = J_2(\sigma_{ij}) = \sqrt{\sigma_{ij}\sigma_{ij}}.$$

This leads still to $A = \sigma_{11}$ since the one-dimensional case is regarded. However, in the one-dimensional loading A remains constant and represents the maximum stress. In analogy for the 3-D case, it is proposed that in Eq. (3.23) also the maximum of A is used, i.e. A can only increase during calculation. This leads to the evolution equation in tensorial form

$$(3.25) \quad \dot{\sigma}_{ij} = \frac{1}{2} D^2 \frac{\sigma_{ij}}{\ln \left[\frac{\sigma_{ij}}{\sup(\sqrt{\sigma_{ij}\sigma_{ij}})} \right]}.$$

3.4. Deformation dependence of diffusion

In the present investigation it is also taken into account that water is pressed out of the specimens during a compressive test, leading to a change in diffusion. For this reason, the diffusion parameter D is treated as a function of the volume strain ε_v :

$$(3.26) \quad D(\varepsilon_v) = D_0 - D_1 |\varepsilon_v|.$$

With this expression, a relation between loss of water and decrease of diffusion is introduced which makes physically sense. Therefore, Eq. (3.26) is used only for negative volume strains. For positive values of ε_v the parameter D is kept constant.

The described derivation leads finally to the following two alternatives of evolution equations for the deformation dependent diffusion process:

$$(3.27) \quad \dot{\sigma}_{ij}^{d1} = -D(\varepsilon_v) \sigma_{ij}$$

and

$$(3.28) \quad \dot{\sigma}_{ij}^{d2} = \frac{1}{2} D^2(\varepsilon_v) \frac{\sigma_{ij}}{\ln \left[\frac{\sigma_{ij}}{\sup(\sqrt{\sigma_{ij}\sigma_{ij}})} \right]},$$

which we call VED1 model and VED2 model, respectively.

3.5. Elastic stiffness distribution

The varying Young's modulus of the specimens has a minimum value E_i and maximum Young's modulus E_m as depicted in Fig. 1. For convenience, the Young's modulus is assumed to be a linear, respectively a quadratic function over the thickness of the specimen. The value E_a stands for the average value of the entire specimen, if it is subjected to pure tension in x -direction. Thus, E_a must be obtained from the quasi-static tension test and is related to E_i and E_m in the form

$$(3.29) \quad E_a = \frac{\int_0^h E(y) dy}{h},$$

with

$$(3.30) \quad E_a = \frac{E_i + E_m}{2} \quad \text{and} \quad E_a = \frac{2}{3} E_i + \frac{1}{3} E_m$$

for the linear and quadratic relationship, respectively.

4. Numerical model

The graded property of the material is taken into account by several layers through the thickness of the specimen. By means of Eqs. (3.29) and (3.30), the Young's modulus $E(y)$, according to Fig. 1, can be determined by the functions

$$(4.1) \quad E(y) = E_i + \frac{E_m - E_i}{h} y \quad \text{and} \quad E(y) = E_i + \frac{E_m - E_i}{h^2} y^2$$

for the linear and quadratic case, respectively.

The stress tensor can now be expressed in incremental form for the VED1 model according to Eqs. (3.12)–(3.14), (3.27) by

$$(4.2) \quad \Delta\sigma_{ij} = C_{ijkl} \Delta\varepsilon_{ij} + \tilde{C}_{ijkl}(\dot{\varepsilon}) \Delta\varepsilon_{ij} - (D_0 - D_1|\varepsilon_v|) \sigma_{ij} \Delta t,$$

with the time increment Δt . In the case of the VED2 model the stress increment is written as

$$(4.3) \quad \Delta\sigma_{ij} = C_{ijkl} \Delta\varepsilon_{ij} + \tilde{C}_{ijkl}(\dot{\varepsilon}) \Delta\varepsilon_{ij} + \frac{1}{2} (D_0 - D_1|\varepsilon_v|)^2 \frac{\sigma_{ij}}{\ln \left[\frac{\sigma_{ij}}{\sup(\sqrt{\sigma_{ij}\sigma_{ij}})} \right]} \Delta t.$$

Due to the rotational symmetry of the cylindrical compression specimens, the numerical model is treated as a two-dimensional problem with plane four-node elements.

5. Material parameter identification

In order to determine the Young's modulus E_a , the curve with the lowest strain rate is assumed to be the quasi-static test. The stress-strain relation of the other curves can be described, according to Eqs. (3.13), (3.14), by

$$(5.1) \quad \sigma_{11} = (E_a + a\dot{\varepsilon}_{11}^v) \varepsilon_{11},$$

with E_a denoting the average Young's modulus (Fig. 1). Here, it is taken into account that the nominal stresses and strains in Fig. 4, measured in the experiments, have to be transformed into true stresses and strains used in the simulations. The nominal strain ε_{11}^0 and nominal stress σ_{11}^0 are calculated by means of the measured elongation $\Delta\ell$, and the force F with respect to the undeformed specimen length ℓ_0 and the undeformed cross-section area A_0 :

$$(5.2) \quad \varepsilon_{11}^0 = \frac{\Delta\ell}{\ell_0}; \quad \sigma_{11}^0 = \frac{F}{A_0}.$$

These quantities can be transformed to true stress and and strain by applying

$$(5.3) \quad \varepsilon_{11} = \ln(1 + \varepsilon_{11}^0); \quad \sigma_{11} = \sigma_{11}^0 (1 + \varepsilon_{11}^0).$$

A Poisson's ratio $\nu = 0.3$ is assumed in order to allow a volume change during deformation. Figure 5 illustrates the reason why to choose a gradient material

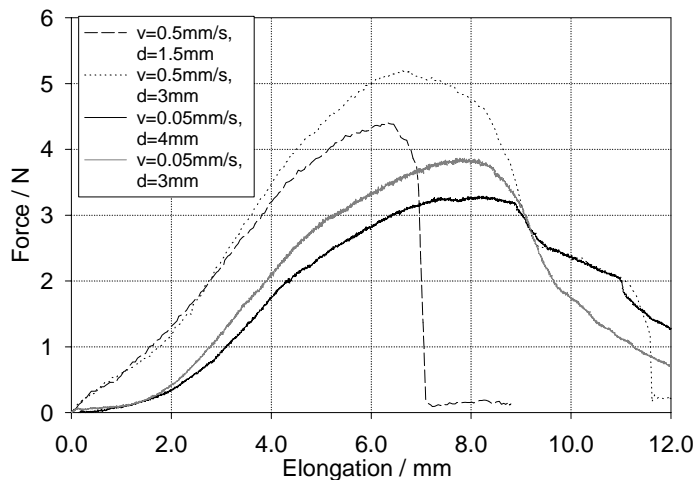


FIG. 5. Tension tests with specimens with different thicknesses.

description: several tension tests at different strain rates are shown with specimens of different thicknesses. One sees that samples with different thicknesses are carrying nearly the same load. This is explained by outer layers of the specimens exhibiting a much higher stiffness than the internal core. The non-linear parts between force and elongation in Fig. 5 have pure experimental reasons. At the beginning of the tests, a force must develop first in the weak material, and at the end a rupture occurs. By means of the tension tests in Fig. 6 the diffusion parameters from Eq. (3.26) can be determined. The tension specimen is first elongated up to 2.5 mm, followed by a rest position in which a decrease of the measured force is visible. If the relaxation behaviour in tension and compression were equal, then the tension test could be used to determine both diffusion parameters D_0 and D_1 . However, in these tension tests it was not observed that liquid was pressed out of the specimens. Consequently, it is assumed that the tension specimen keeps the liquid inside during the test. For this reason, the slope of the force vs. time curve in Fig. 6 is treated as an initial value for the relaxation property. The relaxation curve can be fitted by an exponential function of the form

$$(5.4) \quad F^{d1}(t) = c_1 e^{-D_0 t} + c_2,$$

with $D_0 = 0.4/\text{s}$ belonging to the first kind of viscoelastic diffusion (VED1) from Eq. (3.27). In the case of the second viscoelastic diffusion model (VED2) from Eq. (3.28) the force evolution is expressed as

$$(5.5) \quad F^{d2}(t) = c_3 e^{-D_0 \sqrt{t}} + c_4,$$

leading to $D_0 = 0.62/\sqrt{\text{s}}$ after curve-fitting.

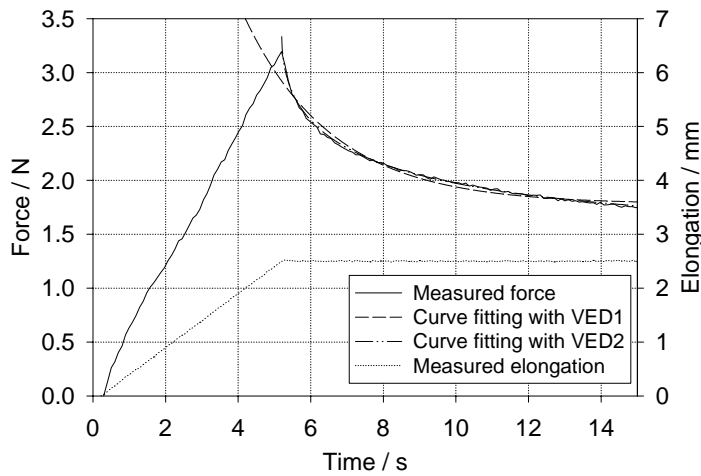


FIG. 6. Tension test with constant elongation causing a relaxation.

6. Simulations and experiments

In Fig. 7 the measured force acting on the compression specimen is shown as well as the measured displacement which is equal to the compression of the sample. The simulated reaction force, acting on the specimen, is the sum of all nodal forces at the lower support of the specimen. Both VED models are used for predicting the internal force in Fig. 7. It can be observed that during the loading path the increase of the reaction force is in good agreement with the measured one. In order to obtain a realistic relaxation curve, the so far unknown parameter D_1 was identified to be equal to $1.1/s$ for the VED1 model and $1.36/\sqrt{s}$ for the VED2 model.

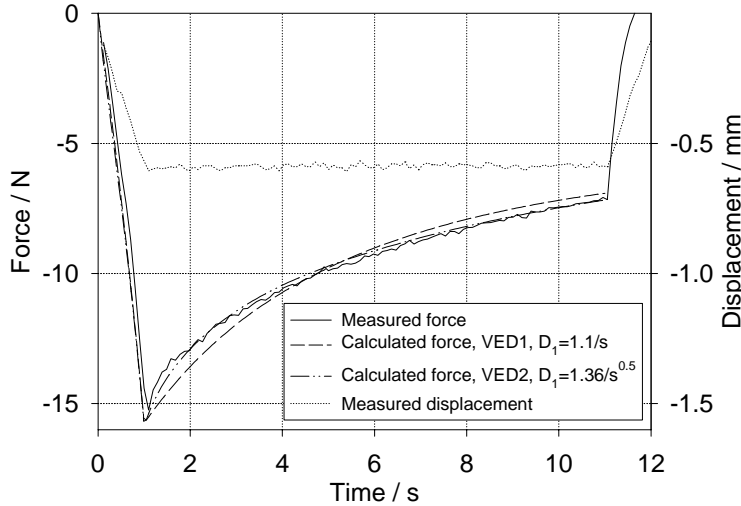


FIG. 7. Compressive test for identifying parameter D_1 .

A realistic peak force in the simulation was achieved by assuming a linear distribution of $E(y)$ with $E_i = 0.1E_a$ for the VED1 model and $E_i = 0.4E_a$ for the VED2 model. As it can be observed in Fig. 7, both approaches of the VED models lead to a good prediction of the measured force. However, results obtained with the VED2 model are significantly closer to the experimental data than those with VED1. Especially, the curvature is predicted better by using the VED2 version. In Figs. 8 and 9 the distributions of the diffusion parameter $D(\varepsilon_v)$ are shown at two different stages of time for VED2. In both pictures, assuming symmetry, only half of the finite element mesh of the collagen specimen is depicted. In Fig. 8 the specimen has reached the maximum compression of 0.6 mm after 1 s, see Fig. 7. From the legend it can be seen that in the outer zones of the specimen, the initial value of $D_0 = 0.62/\sqrt{s}$ is nearly still valid.

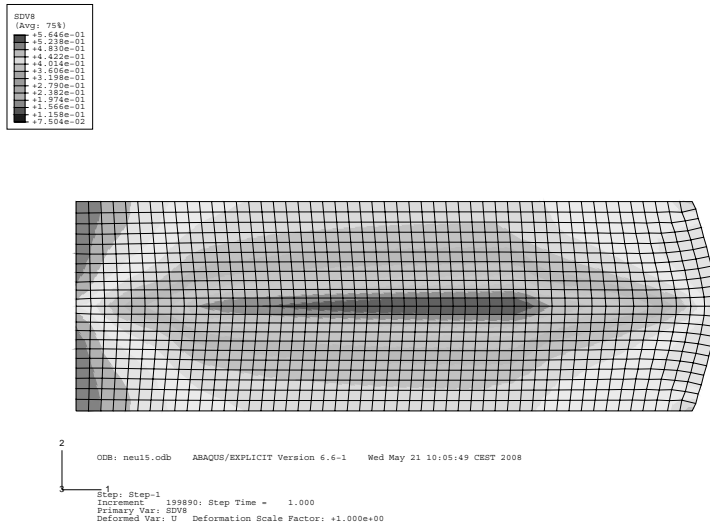


FIG. 8. Deformed finite element mesh with distribution of the diffusion parameter at time $t = 1$ s (start of relaxation).

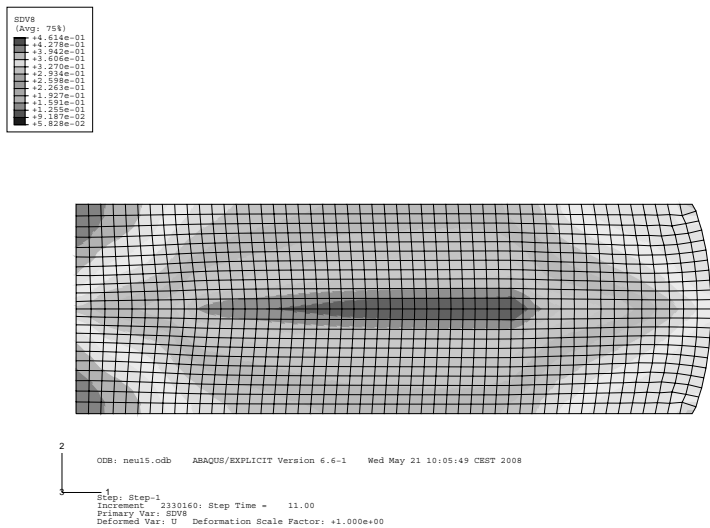


FIG. 9. Deformed finite element mesh with distribution of the diffusion parameter at time $t = 11$ s (end of compression).

In Fig. 9 the deformed mesh is shown at time $t = 11$ s, i.e. at the end of the simulation in Fig. 7, and D has decreased to approximately $0.4/\sqrt{s}$ in the outer zones. This effect covers the propagation of liquid due to volume change and has an important influence on the evolution of stresses and, hence, on the relaxation process.

7. Discussion

After all diffusion parameters have been identified, another comparison between simulation and experiment with both types of VED and a new sample of the same condensation level is presented in Fig. 10. For this specimen a quadratic function of $E(y)$ with $E_i = 0.25E_a$ for VED1 and $E_i = 0.35E_a$ for VED2 is assumed. In Fig. 10 three calculated forces are shown. Two force evolutions with VED1 and VED2 were obtained by using the same values for D_1 as in Fig. 7. Here, the predicted force by using VED1 is in better correlation with the measurement than the simulation by applying VED2. In the case of VED2 a modification of the diffusion coefficient to $D_1 = 1.51/\sqrt{s}$ is necessary to obtain a good agreement with the measured force in which also the curvature of the curve is predicted again precisely. Consequently, it can be summarized that the simulation with the VED1 model and the determined parameter $D_1 = 1.1/s$ from Fig. 7 still predicts the measurement well. However, the calculated force by means of the VED2 model is quite sensitive to a variation of the Young's modulus distribution and, hence, leads to a divergence from the experiment. This can be due to the non-linear stress terms in the diffusion part in Eq. (4.3) causing a higher sensitivity with respect to parameter variations as in Eq. (4.2). A variation in the diffusion property of the material could not be the reason for the change of the parameter D_1 in the VED2 model, because in this case the value of D_1 for the VED1 law would vary, too.

Concerning the material parameter identification process it can be concluded that all viscous parameters and the average Young's modulus E_a can be obtained

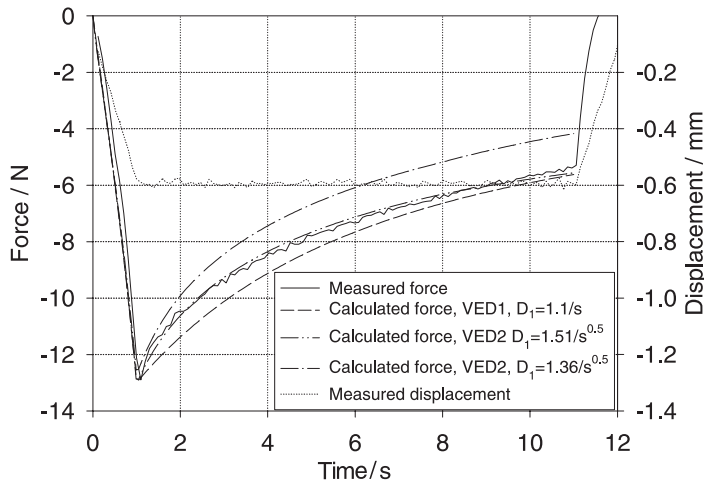


FIG. 10. Validation of identified diffusion parameters D_1 .

by tension tests. However, the remaining values, which have to be determined by finite element simulations are the internal Young's modulus E_i and the diffusion coefficient D_1 .

8. Conclusions

The investigated condensed collagen material showed clear strength and damping properties which are important for a cartilage replacement material. Due to the good correlation between measurements and simulations, the proposed model is supposed to be applicable to collagen gel materials. The VED2 model which includes the \sqrt{t} -law leads to the best predictions of simulated internal forces compared to measurements. However, the VED1 model exhibits a lower sensitivity to material parameter variations. By means of separate tension tests it was possible to identify all material parameters, with exception of internal Young's modulus and a diffusion parameter which had to be determined by numerical parameter identification.

Acknowledgment

The authors would like to thank Prof. Dr.-Ing. Josef Betten, Mathematical Models in Materials Science and Continuum Mechanics, RWTH Aachen, for his remarks and helpful discussions.

References

1. W. EHLERS, B. MARKERT, *A linear viscoelastic biphasic model for soft tissues based on the theory of porous media*, Transactions of ASME, **123**, 418–424, 2001.
2. M.R. DI SILVESTRO, Q. ZHU, M. WONG, J.S. JURVELIN, J.-K.F. SUH, *Biphasic poroviscoelastic simulation of the unconfined compression of articular cartilage: I – Simultaneous prediction of reaction force and lateral displacement*, J. Biomechanical Eng., **123**, 191–197, 2001.
3. J.J. GARCÍA, D.H. CORTÉS, *A nonlinear biphasic viscohyperelastic model for articular cartilage*, J. Biomechanics, **39**, 2991–2998, 2006.
4. J.J. GARCÍA, D.H. CORTÉS, *A biphasic viscohyperelastic fibril-reinforced model for articular cartilage: Formulation and comparison with experimental data*, J. Biomechanics, **40**, 1737–1744, 2007.
5. W. WILSON, C.C. VAN DONKELAAR, B. VAN RIETBERGEN, R. HUISKES, *A fibril-reinforced poroviscoelastic swelling model for articular cartilage*, J. Biomechanics, **38**, 1195–1204, 2005.
6. M.A. HAIDER, R.C. SCHUGART, *A numerical method for the continuous spectrum biphasic poroviscoelastic model of articular cartilage*, J. Biomechanics, **39**, 177–183, 2006.

7. F. GUILAK, V.C. MOW, *The mechanical environment of the chondrocyte: a biphasic finite element model of cell-matrix interactions in articular cartilage*, J. Biomechanics, **33**, 1663–1673, 2000.
8. X.N. MENG, M.A. LEROUX, T.A. LAURSEN, L.A. SETTON, *A nonlinear finite element formulation for axisymmetric torsion of biphasic materials*, Int. J. Solids and Structures, **39**, 879–895, 2002.
9. V.C. MOW, S.C. KUEI, W.M. LAI, C.G. ARMSTRONG, *Biphasic creep and stress relaxation of articular cartilage in compression: theory and experiments*, J. Biomechanical Eng., **102**, 73–84, 1980.
10. E.M. JOHNSON, W.M. DEEN, *Hydraulic permeability of agarose gels*, AIChE Journal, **42**, 1220–1224, 1996.
11. W.Y. GU, H. YAO, C.Y. HUANG, H.S. CHEUNG, *New insight into deformation-dependent hydraulic permeability of gels and cartilage, and dynamic behavior of agarose gels in confined compression*, J. Biomechanics, **36**, 593–598, 2003.
12. F. LEI, A.Z. SZERI, *Inverse analysis of constitutive models: Biological soft tissues*, J. Biomechanics, **40**, 936–940, 2007.
13. J.E. OLBERDING, J.-K.F. SUH, *A dual optimization method for the material parameter identification of a biphasic poroviscoelastic hydrogel: Potential application to hypercompliant soft tissues*, J. Biomechanics, **39**, 2468–2475, 2006.
14. M.H. HOLMES, V.C. MOW, *The nonlinear characteristic of soft gels and hydrated connective tissues in ultrafiltration*, J. Biomechanics, **23**, 1145–1156, 1990.
15. T. COURTNEY, M.S. SACKS, J. STANKUS, J. GUAN, W.R. WAGNER, *Design and analysis of tissue engineering scaffolds that mimic soft tissue mechanical anisotropy*, Biomaterials, **27**, 3631–3638, 2006.
16. G.C. ENGELMAYR JR., G.D. PAPWORTH, S.C. WATKINS, J.E. MAYER JR., M.S. SACKS, *Guidance of engineered tissue collagen orientation by large-scale scaffold microstructures*, J. Biomechanics, **39**, 1819–1831, 2006.
17. B.E. KOOP, J.L. LEWIS, *A model of fracture testing of soft viscoelastic tissues*, J. Biomechanics, **36**, 605–608, 2003.
18. J.F. RODRÍGUEZ, F. CACHO, J.A. BEA, M. DOBLARÉ, *A stochastic-structurally based three-dimensional finite-strain damage model for fibrous soft tissue*, J. Mechanics Physics of Solids, **54**, 864–886, 2006.
19. Y.C. FUNG, *Biomechanics: Mechanical properties of living tissue*, Springer, New York, 1993.
20. G.A. HOLZAPFEL, T.C. GASSER, R.W. OGDEN, *A new constitutive framework for arterial wall mechanics and a comparative study of material models*, J. Elasticity, **61**, 1–48, 2000.
21. A.E. EHRET, M. ITSKOV, *A polyconvex hyperelastic model for fiber-reinforced materials in application to soft tissues*, J. Mater. Sci., **42**, 8853–8863, 2007.
22. E.J. WEINBERG, M.R. KAAZEMPUR-MOFRAD, *A large-strain finite element formulation for biological tissues with application to mitral valve leaflet tissue mechanics*, J. Biomechanics, **39**, 1557–1561, 2006.

23. J.E. BISCHOFF, *Continuous versus discrete (invariant) representations of fibrous structure for modeling non-linear anisotropic soft tissue behavior*, Int. J. Non-Linear Mech., **41**, 167–179, 2006.
24. T.E. SAYED, A. MOTA, F. FRATERNALI, M. ORTIZ, *A variational constitutive model for soft biological tissues*, J. Biomechanics, in press.
25. W. ZHANG, H.Y. CHEN, G.S. KASSAB, *A rate-insensitive linear viscoelastic model for soft tissues*, Biomaterials, **28**, 3579–3586, 2007.
26. K.Y. VOLOKH, *Prediction of arterial failure based on a microstructural bi-layer fiber-matrix model with softening*, J. Biomechanics, **41**, 447–453, 2008.
27. L. ZHANG, A.Z. SZERI, *Transport of neutral solute in articular cartilage: Effect of microstructure anisotropy*, J. Biomechanics, **41**, 430–437, 2008.
28. K. MILLER, K. CHINZEI, *Mechanical properties of brain tissue in tension*, J. Biomechanics, **35**, 483–490, 2002.
29. J. LEPETIT, R. FAVIER, A. GRAJALES, P.O. SKJERVOLD, *A cryogenic holder for tensile testing of soft biological tissues*, J. Biomechanics, **37**, 557–562, 2004.
30. J.Z. WU, R.G. DONG, A.W. SCHOPPER, *Analysis of effects of friction on the deformation behavior of soft tissues in unconfined compression tests*, J. Biomechanics, **37**, 147–155, 2004.
31. C. JAQUEMOUD, K. BRUYERE-GARNIER, M. CORET, *Methodology to determine failure characteristics of planar soft tissues using a dynamic tensile test*, J. Biomechanics, **40**, 468–475, 2007.
32. D.-L. GUO, B.-S. CHEN, N.-S. LIU, *Investigating full-field deformation of planar soft tissue under simple-shear tests*, J. Biomechanics, **40**, 1165–1170, 2007.
33. T.J. KLEIN, M. CHAUDHRY, W.C. BAE, R.L. SAH, *Depth-dependent biomechanical and biochemical properties of fetal, newborn, and tissue-engineered articular cartilage*, J. Biomechanics, **40**, 182–190, 2007.
34. H. SARAF, K.T. RAMESH, A.M. LENNON, A.C. MERKLE, J.C. ROBERTS, *Mechanical properties of soft human tissues under dynamic loading*, J. Biomechanics, **40**, 1960–1967, 2007.
35. M.J. KOEHLE, M.L. HULL, *A method of calculating physiologically relevant joint reaction forces during forward dynamic simulations of movement from an existing knee model*, J. Biomechanics, **41**, 1143–1146, 2008.
36. K. MILLER, *Method of testing very soft biological tissues in compression*, J. Biomechanics, **38**, 153–158, 2005.
37. J. BETTEN, *Creep Mechanics*, Springer, Berlin Heidelberg, New York 2005.

Received November 4, 2008; revised version January 20, 2009.
